An investigation of phase transformation and crystallinity in laser surface modified H13 steel

S.N. Aqida · D. Brabazon · S. Naher

Abstract

This paper presents a laser surface modification process of AISI H13 tool steel using 0.09, 0.2 and 0.4 mm size of laser spot with an aim to increase hardness properties. A Rofin DC-015 diffusion-cooled CO_2 slab laser was used to process AISI H13 tool steel samples. Samples of 10 mm diameter were sectioned to 100 mm length in order to process a predefined circumferential area. The parameters selected for examination were laser peak power, overlap percentage and pulse repetition frequency (PRF). X-ray diffraction analysis (XRD) was conducted to measure crystallinity of the laser-modified surface. X-ray diffraction patterns of the samples were recorded using a Bruker D8 XRD system with CuK_α ($\lambda = 1.5405$ Å) radiation. The diffraction patterns were recorded in the 2θ range of 20 to 80°. The hardness properties were tested at 981 mN force. The lasermodified surface exhibited reduced crystallinity compared to the un-processed samples. The presence of martensitic phase was detected in the samples processed using 0.4 mm spot size. Though there was reduced crystallinity, a high hardness was measured in the laser-modified surface. Hardness was increased more than 2.5 times compared to the as-received samples. These findings reveal the phase source of the hardening mechanism and grain composition in the laser-modified surface.

1. Introduction

In laser surface processing, formation of a modified layer is determined by the laser parameter settings. Some laser parameters are laser beam wavelength, temporal pulse power (pulse length, peak power and pulse shape), repetition rate, beam energy distribution, and beam geometry including focal spot size and depth of focus [1]. Control of parameter settings also yields different effects on the modified surface properties. Increasing the laser power increases the surface temperature, which influences the molten surface solidification rate. While a high cooling rate is necessary to refine the grain structures, a high power density and short interaction time combination is generally preferred to allow for a faster cooling rate to be achieved. The modified layer could exhibit high hardness from the formation of finer grains, secondary carbide and hard non-equilibrium microstructures that are intimately bonded to the substrate and the modified region itself [2, 3].

Rapid solidification from laser processing usually results in supercooled melt and phase transformation in metal alloys [4–6]. In laser-treated stainless steel samples, a decrease of α-Fe peak intensity and a typical martensite–austenite phase transformation were detected after laser treatment at a power density of 1.02×10^9 W/m^2, while a full transformation to austenite phase occurred when processed at 1.45×10^9 W/m^2 power density [7]. A similar effect occurred in a laser melted high chrome steel surface where fast quenching of the laser melted

sample yielded austenite phase [6]. Peak broadening has also been attributed to the existence of fine grain size and stress on the materials surface in stainless steel samples [7]. However, though much work has discussed the phase transformation in laser processed steel, very little work focussed on the formation of quasicrystalline phase and its relation to hardness properties. This work highlights hardening mechanism of lasermodified surface, and phase transformation in supercooled austenite. In this paper, metastable phase and phase crystallinity of laser-modified H13 steel surface were investigated.

2. Experimental

The material investigated in this study was H13 die steel with chemical composition of alloying elements given as 0.32–0.45 wt.% C, 0.20–0.50 wt.% Mn, 0.80–1.20 wt.% Si, 4.75–5.50 wt.% Cr, 0.30 wt.% Ni, 1.10–1.75 wt.% Mo,0.80–1.20 wt.% V, 0.25 wt.% Cu, 0.03 wt.% P and S.

As-received 10 mm diameter H13 die steel cylindrical rods were sectioned into 120 mm length samples. The samples were cleaned with ethanol prior to processing. Samples were laser processed after surface roughening to produce 3.0 ± 0.2 µm average roughness and then were chemically etched. A Rofin DC-015 diffusion-cooled CO_2 slab laser system with 10.6 µm wavelength was used to modify the sample surface. The laser system was focussed to a minimum laser spot diameter of 0.09 mm onto the sample surface, and was defocussed from its focal position to a focal position above the surface to achieve a larger laser surface beam spot diameter of 0.2 and 0.4 mm. The beam mode was TEM_{oo}, which produced a fine circular beam size. Table 1 shows the parameter settings used to process the samples with three different spot sizes.

The parameters used were peak power, P_p, duty cycle, DC, overlap, η, and pulse repetition frequency, PRF. The duty cycle was based on peak power to result in a range of average power. In pulse mode processing, overlap was set to produce a continuous effect of modified surface, which was achieved by either increasing the laser PRF at constant sample translation speed or by changing sample translation speed at constant PRF. Overlapped pulse in E samples were designed using the first technique while the latter calculation was conducted in N and X samples. The outcome parameters from the settings were residence time, T_R, irradiance, I, and pulse energy, E_p.

Table 1 Laser processing parameters

Set parameters	Sample					
	E8	E15	N4	N12	X2	X5
P_p (W)	760	760	507	1313	1138	1138
DC (%)	85	100	49	23	24	24
η (%)	10	30	50	50	0	10
PRF (Hz)	2857	3810	2900	2900	2900	2900
Outcome parameters						
I (W/mm^2)	5,548	4,631	10,930	28,184	178,761	162,572
T_R (ms)	0.32	0.34	0.25	0.12	0.08	0.09
E_p (J)	0.23	0.20	0.09	0.11	0.10	0.10

These parameters were calculated using Eqs. 1, 2 and 3:

$$T_R = \frac{DC \times d}{S} \tag{1}$$

$$I = \frac{F}{T_R} \times DC \tag{2}$$

$$E = \frac{P_{ave}}{PRF} \tag{3}$$

where d is laser spot diameter, F is energy density (pulse energy divided by laser beam spot area), S is traverse speed (laser spot diameter divided by time taken to produce one rotation) and P_{ave} is average power (peak power multiply with duty cycle).
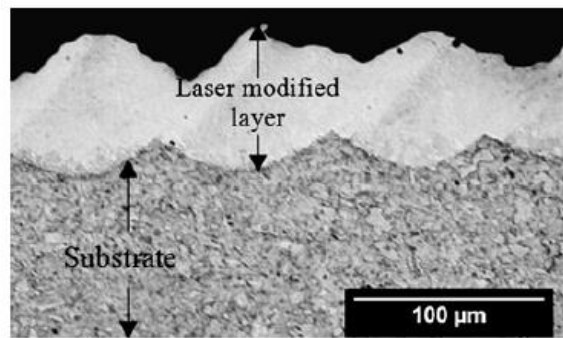

Fig. 1 Micrograph of laser-modified surface cross section (sample N12)

Micrograph of laser-modified surface cross section was observed using EVO-LS15, Carl Zeiss, scanning electron microscope (SEM) integrated with SmartSEM software. X-ray diffraction patterns of the samples were recorded using a Bruker D8 XRD system with Cu K$_\alpha$ (λ = 1.5405 Å) radiation. The hardness properties were tested at 981 mN force using Leitz mini-load tester with Vickers diamond indenter.

3. Results

The laser-modified layer produced on H13 steel substrate of sample N12 is shown in Fig. 1. The laser-modified surface H13 was analysed for surface crystallinity and compared with the diffraction pattern of the as-received H13 steel. In Fig. 2, the diffraction peaks of as-received H13 steel surface were characterised by distinct reflections of α-Fe (110) , (200), (211) and (220) phase at 44.6∘, 64.8∘, 82.1∘ and 98.6∘ Bragg's angles (2 theta), respectively. The intensity distribution of the peaks was similar to the α-Fe phase (06-0696) peaks listed in the Joint Committee on Powder Diffraction Standards (JCPDS) database.

The X-ray diffraction patterns produced by samples processed at 0.4, 0.2 and 0.09 mm spot size are shown in Figs. 3, 4 and 5, respectively.

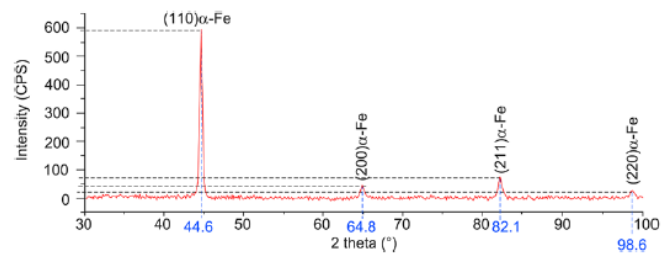**Fig. 2** X-ray diffraction pattern of as-received H13 tool steel

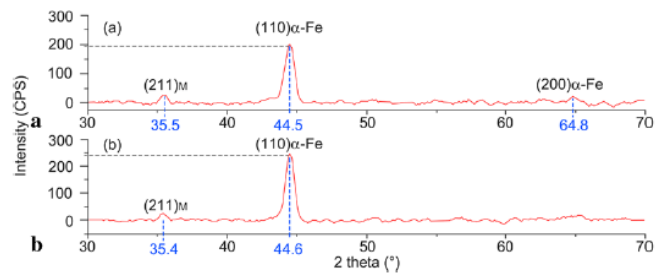**Fig. 3** X-ray diffraction patterns of (**a**) E15 and (**b**) E8 sample processed at 0.4 mm spot size

Fig. 4 X-ray diffraction patterns of (**a**) N4 and (**b**) N12 sample processed at 0.2 mm spot size
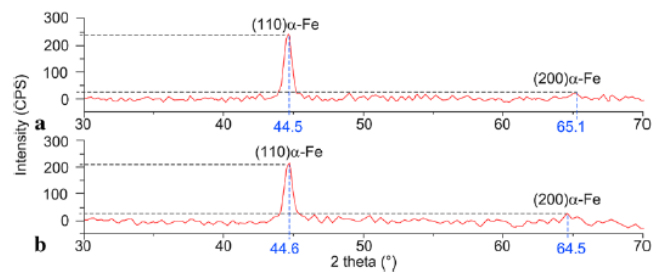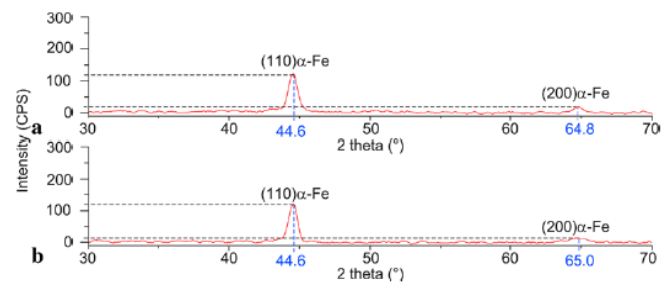

Fig. 5 X-ray diffraction patterns of (**a**) X5 and (**b**) X2 sample processed at 0.09 mm spot size

The peaks detected from Fig.3(a) were (211) martensite, (110) and (200) α-Fe. Whereas in Fig. 3(b) the (200) α-Fe peak became less distinct and suppressed. At 0.4 mm spot size, the (110) α-Fe phase peak in Fig. 3(a) decreased as much as 66 % (from approximately 600 to 200 cps) compared to the as-received H13 steel surface peak reflection, see Fig. 2. Presence of (211) martensite peak was detected at 35.45° Bragg's angle, see Fig. 3. The (211) martensite structure is body-centred-cubic in contrast with as-quenched martensite body-centred-tetragonal structure.

In Figs. 4(a) and (b), samples processed at 0.2 mm spot size produced (110) α-Fe peaks at 60 % lower intensity than the as-received H13, which reduced from approximately 600 to 230 cps. The (200) α-Fe peak for samples in Fig. 4(a) decreased approximately 50 % compared to the as-received H13 tool steel. Further (110) α-Fe peak reduction was observed on diffraction patterns of samples processed at a 0.09 mm spot size as shown in Figs. 5(a) and (b). The peak intensity of (110) α-Fe resulted from an as-received H13 sample was more than four times stronger compared to samples in Fig. 5. A broadening effect of (200) α-Fe peak was found in the sample of Fig. 5(b).

The crystallinity of the laser-modified H13 tool steel sample surfaces were different from the as-received H13 steel in terms of relative strength ratio, I/I_1, of diffraction peaks. Detailed results of X-ray diffraction values for characterised angle measured from the samples scanning patterns and the standard peaks of α-Fe from the JCPDS database are given in Table 2.

Table 2 Contrast of x-ray diffraction values for as-received H13 and laser-modified H13 steel surface

Sample/spot size (mm)	Measured values					Data from JCPDS (α-Fe: 06-0696)		
	2θ (°)	Max. intensity (CPS)	d (nm)	I/I_1	FWHM (2θ)	d (nm)	I/I_1	Plane (hkl)
As-received H13	44.6	591.0	0.2031	100	0.342	0.2027	100	110
	64.8	43.2	0.1437	7	0.584	0.1433	20	200
	82.1	72.8	0.1173	12	0.598	0.1170	30	211
E15/0.4	35.5	24.6	0.2530	12	0.607			
	44.5	199.4	0.2035	100	0.854			
	64.8	19.7	0.1438	10	0.692			
E8/0.4	35.4	25.4	0.2530	10	0.601			
	44.6	243.6	0.2036	100	0.861			
N12/0.2	44.5	233.4	0.2033	100	0.849			
	65.1	20.6	0.1431	9	1.962			
N4/0.2	44.6	233.0	0.2033	100	0.925			
	64.5	36.5	0.1443	16	1.969			
X5/0.09	44.6	123.0	0.2032	100	0.940			
	64.8	12.3	0.1438	10	n/a			
	82.2	30.8	0.1172	25	n/a			
X2/0.09	44.6	131.0	0.2031	100	1.045			
	64.3	12.3	0.1448	9	n/a			
	82.2	26.9	0.1172	21	n/a			

The peaks' angles associated with as-received H13 steel surface were compared with the modified samples. All of the peaks detected on modified samples were at similar angles of reflection as the asreceived H13 sample. The inter-planar spacing, d of the modified samples was retained while the relative intensity strengths differed. Referring to α-Fe (06-0696) from the JCPDS database, the relative strength ratio of the peaks at the four different angles were 100, 20, 30 and 10. The (200) α-Fe peak was diminished in sample E8 while it became more distinct in sample N12. Sample E8 processed at 0.4 mm spot size produced the (211) martensite peak at 35.4° with at least 10 % of the relative strength ratio. The relative strength ratio of (211) α-Fe peak in sample X2 and X5 was higher than the as-received H13 steel (see Table 2). The FWHM values of (110) α-Fe peak in samples E8, E15, N4 and N12 increased at least 2.5 times higher than in asreceived H13 steel. In sample X5, the increment was 2.7 times. A broadening of 1.045° was analysed on (200) α-Fe peak of sample X2, which was three times that of the asreceived H13 peak.

The resulted maximum hardness of laser-modified surface processed at 0.09, 0.2 and 0.4 mm spot size are 824, 996 and 1017 $HV_{0.1}$, respectively. The highest average hardness was measured in sample processed using 0.4 mm spot size. The sample N4, which was processed at 0.2 mm spot size, exhibited the lowest peak hardness of 435 $HV_{0.1}$.

4. Discussion

The peak reflection analysis of the modified samples conducted between 30 to 70° Bragg's angle was sufficient to investigate the phase crystallinity and broadening effect of the (110)

α-Fe phase. The α-Fe phase expresses super saturation solid solution martensite and ferrite [8]. Peak reduction occurred in all laser-modified samples with maximum reduction in samples X2 and X5 shown in Fig. 5. Since sharp and strong peaks show a well-crystalline nature of α-Fe phase, the peak intensity reductions resulted from decreasing phase crystallinity [9]. The finding on decreasing phase crystallinity also supports the supercooled austenite transformation discussion earlier.

Referring to the processing parameter effects on samples in Table 2, the smaller spot size of 0.09 mm resulted in a more rapid heating rate compared to 0.2 and 0.4 mm spot size due to the combination of settings of high irradiance and short exposure time. Longer exposure times were necessary when processing samples at low laser irradiance to allow surface melting to take place. A low heating rate and small undercooling interplay in sample E8 and E15 to produce martensite phase during processing, see Fig. 3. A similar peak traced at 35° angle position was referred to as structural transformation in water quenched Fe–Ga alloys after being heat treated at 1000 °C [10]. At 4,600 W/mm^2 laser irradiance and 0.34 ms exposure time, the (110) and (200) α-Fe crystalline peaks intensity of sample E15 were reduced, see Fig. 3(a). A small increase of heating rate (5,548 W/mm^2 laser irradiance and 0.32 ms exposure time) was adjusted for sample E8, which suppressed the (200) α-Fe peak, see Fig. 3(b).

In Table 1, the laser irradiances for sample N4 and N12 were 10,930 W/mm^2 and 28,184 W/mm^2 with residence times of 0.25 and 0.12 ms, respectively. The martensite peak was absent in both samples N4 and N12. A noticeable change was the intensity of the (200) α-Fe peak decreased 10 % more in sample N12 in contrast to N4 due to higher laser irradiance. The samples processed at spot size of 0.09 mm indicated the presence of a small amount of randomly distributed nano-subgrains in the laser-modified surface from the decrease of the crystalline peak intensity. The findings show significant effect of heating rate where at low irradiance and longer exposure time combination, the martensitic transformation was initiated. Whereas the large undercooling allowed for the martensitic transformation to be skipped and suppressed several long range order peaks. More rapid cooling occurred in smaller laser spot size due to lower residence time, which limited the heat transfer to the surface.

The formation of nano size and ultrafine size grain structures in the modified layer corresponds to the diffraction peak intensities found in the XRD analysis which can be referred to authors' previous findings [11]. A small broadening effect occurred in the diffracted peaks of the modified surface due to an increase of grain boundaries from ultrafine size subgrain formations. In sample E15 and E8, one of the factors which caused grain refinement was the growth and evolution of martensite phase due to grain- subgrain boundaries and lattice structure changes under the specific variation in temperature [12, 13]. The broadening effect investigated is also correlated with the mechanical properties of steel where ultrafine grain exhibits high strength and good ductility in metallic materials [14, 15].

Increment of hardness properties in samples processed by 0.4 mm spot size was contributed to by grain refinement along with martensite phase presence, which is in agreement with the XRD findings and previous work [16].

The pulse energy and residence time combination determines the surface heating rate and quench rate of undercooled austenite. The smaller spot size of 0.2 mm compared to the 0.4 mm spot size yielded higher irradiance and retained stress during surface processing. A vast difference between sample N12 and N4 average hardness was due to changes in both the peak and average power settings. The hardness measured in sample processed at 0.11 J pulse energy indicates that a finer grain size ferrite was transformed from undercooled austenite at this higher irradiance and shorter residence time setting. Even though a lower irradiance needs a longer residence time for surface melting, however, for grain refinement, the grain size depends on the cooling period and the effect of both irradiance and residence time setting on the sample surface temporal temperature.

5. Conclusion

A significant decrease of α-Fe crystallinity and development of metastable phases were identified in the laser-modified surface. Decreasing phase crystallinity and phase transformation variation in the laser-modified surface was dependant on processing parameter settings, in particular the laser spot size. Processing H13 tool steel samples using a laser spot size of 0.4 mm yielded martensite phase. Absence of martensite phase in samples processed at 0.2 and 0.09 mm laser spot size was due to the higher cooling rate on the sample surface. The laser-modified surface hardness properties were enhanced to greater than three times higher than the unmodified H13 tool steel substrate in the DOEs. Increase of hardness due to grain size decrease was in agreement with the Hall–Petch relationship. The laser irradiance and residence time variations at three different laser spot sizes used in the processing were suitable to enhance the surface hardness. These findings reveal the phase source of the hardening mechanism and grain composition in the laser-modified surface.

References

1. F.O. Olsen, L. Alting, Manuf. Technol. **44**, 141 (1995)
2. R.J. DiMelfi, P.G. Sanders, B. Hunter, Surf. Coat. Technol. **106**, 30 (1998)
3. SeDao, M. Hua, T.M. Shao, H.Y. Tam, J. Mater. Process. Technol. **209**, 4689 (2009)
4. R. Roy, S. Gedevanishvili, E. Breval, P. Mistry, M. Turchan, Mater. Lett. **46**, 30 (2000)
5. F. Audebert, R. Colaço, R. Vilar, H. Sirkin, Scr. Mater. **48**, 281 (2003)
6. M. Li, Y. Wang, B. Han, W. Zhao, T. Han, Appl. Surf. Sci. **255**, 7574 (2009)
7. C. Cui, J. Hu, Y. Liu, K. Gao, Z. Guo, Appl. Surf. Sci. **254**, 6779 (2008)
8. L. Yajiang, W. Juan, Z. Bing, F. Tao, Bull. Mater. Sci. **25**, 213 (2002)
9. F. Wang, A. Shan, X. Dong, J. Wu, Scr. Mater. **56**, 737 (2007)
10. T.A. Lograsso, A.R. Ross, D.L. Schlagel, A.E. Clark, M. WunFogle, J. Alloys Compd. **350**, 95 (2003)

11. S.N. Aqida, S. Naher, D. Brabazon, AIP Conf. Proc. **1353**, 1081 (2011)
12. E. Yasar, H. Gungunes, S. Akturk, T.N. Durlu, J. Alloys Compd. **428**, 125 (2007)
13. A.S.J. Suiker, S. Turteltaub, Philos. Mag. **87**, 5033 (2007)
14. M. Brezenitsky, R. Moreh, D. Dayan, G. Kimmel, J. Alloys Compd. **290**, 257 (1999)
15. M. Movaghar Garabagh, S. Hossein Nedjad, M. Nili Ahmadabadi, J. Mater. Sci. **43**, 6840 (2008)
16. M. Eroglu, M. Aksoy, Mater. Sci. Eng. A, Struct. Mater.: Prop. Microstruct. Process. **286**, 289 (2000)